

# Nanohydrodynamics: The Intrinsic Flow Boundary Condition on Smooth Surfaces<sup>†</sup>

Cécile Cottin-Bizonne,<sup>‡</sup> Audrey Steinberger,<sup>‡</sup> Benjamin Cross,<sup>‡</sup> Olivier Raccurt,<sup>§</sup> and Elisabeth Charlaix<sup>\*‡</sup>

Université de Lyon, F-69003 Lyon, Laboratoire PMCN Université Lyon 1, CNRS UMR5586 F-69622, Villeurbanne, France, and CEA-LITEN, Department of Nano-Material, 17 avenue des Martyrs, F-38054 Grenoble, France

Received August 8, 2007. In Final Form: December 3, 2007

A dynamic surface force apparatus is used to determine the intrinsic flow boundary condition of two simple liquids, water and dodecane, on various smooth surfaces. We demonstrate the impact of experimental errors and data analysis on the accuracy of slip length determination. In all systems investigated, the dissipation is described by a well-defined boundary condition accounting for a whole range of separation, film thickness, and shear rate. A no-slip boundary condition is found in all wetting situations. On strongly hydrophobic surfaces, water undergoes finite slippage that increases with hydrophobicity. We also compare the relative influence of hydrophobicity and liquid viscosity on boundary flow by using water–glycerol mixtures with similar wetting properties.

## 1. Introduction

Growing applications involving flows at small scales or in confined geometries, such as liquid transport in mesoporous media, micro- or nanofluidics devices, flows in electrostatic double layers, and biolubrication flows, have raised interest in a precise description of the transport properties of liquids near a solid surface. Beyond applications in narrow channels, in which low friction at a wall would allow the reduction of pressure drops as well as the hydrodynamic dispersion of transported species, the interplay between surface interactions and interfacial hydrodynamics offers a wide range of opportunities to tune and improve the manipulation of matter on the colloidal scale. Examples are electrokinetic phenomena or diffusiophoresis, where the possibility of liquid slippage at a wall can drastically enhance the velocities induced by the externally applied fields.<sup>1</sup>

The first investigation of boundary flows performed with a subnanometer resolution was made in the 1980s with the surface forces apparatus.<sup>2,3</sup> These experiments have brought about experimental evidence supporting the validity of the no-slip boundary condition on the molecular scale for various liquids on atomically smooth mica surfaces.

More recently, this validity has been challenged by new experiments. A variety of experimental methods have been devised to study flows at interfaces, including colloidal probe AFM,<sup>4</sup> fluorescence recovery after photobleaching<sup>5</sup> and fluorescence correlation techniques,<sup>6</sup> micro-PIV,<sup>7</sup> microfluidic pressure drops,<sup>8</sup> and the diffusion of confined colloids.<sup>9</sup> It is now recognized that the no-slip boundary condition (bc) may not always apply to liquid flows past solid boundaries. A partial slip

boundary condition is usually described using the so-called slip length or Navier length  $b$ , which yields, for Newtonian liquids,

$$V_s = b\dot{\gamma}_{\text{wall}} \quad (1)$$

where  $V_s$  is the slip velocity of the liquid and  $\dot{\gamma}_{\text{wall}}$  is the shear rate at the wall. The amplitude of the intrinsic slip of simple liquids on smooth solid surfaces, its variation with the liquid properties, surface characteristics, and flow parameters, are currently matters of active debate.<sup>10,11</sup>

Here we use a dynamic surface force apparatus (DSFA) specifically designed for nanorheology experiments, to determine the bc at the solid/liquid interface. The article is organized as follows. Section 2 describes our experimental technique and discusses the resolution in the bc determination. Section 3 describes the materials and methods. Section 4 presents our results for the boundary flow of two simple liquids, water and dodecane, on low roughness surfaces of various wettabilities. We also investigate the effect of the liquid viscosity by using water–glycerol mixtures, of similar wetting properties on the same hydrophobic surface. In section 5, we compare our results to other experimental work using SFA or colloidal probe AFM. We show that depending on the method used for data analysis, minute inaccuracy in the measurement of the separation can result in very large errors in the slip length. We also compare our data to available theoretical results and molecular dynamic simulations of the intrinsic bc at the liquid/solid interface.

## 2. Experimental Method

### 2.1. Drainage of a Liquid Film between a Sphere and a Plane.

The experimental method uses the viscous force induced by the drainage of a liquid confined between a sphere and a plane in order to determine the bc onto the surfaces. This general method is common both to the surface force apparatus and to the colloidal probe AFM.

<sup>†</sup> Part of the Molecular and Surface Forces special issue.

<sup>\*</sup> To whom correspondence should be addressed. E-mail: elisabeth.charlaix@univ-lyon1.fr.

<sup>‡</sup> Université de Lyon.

<sup>§</sup> CEA-LITEN.

(1) Ajdari, A.; Bocquet, L. *Phys. Rev. Lett.* **2006**, *96*, 18, 186102.

(2) Chan, D. C. Y.; Horn, R. G. *J. Chem. Phys.* **1985**, *83*, 5311.

(3) Israelachvili, J. N. *J. Colloid Interface Sci.* **1986**, *110*, 263.

(4) Sun, G.; Bonaccorso, E.; Franz, V.; Butt, H.-J. *J. Chem. Phys.* **2002**, *117*, 10310–10314.

(5) Pit, R.; Hervet, H.; Léger, L. *Tribol. Lett.* **1999**, *7*, 147.

(6) Lumma, D.; Best, A.; Gansen, A.; Feuillebois, F.; Radler, J. O.; Vinogradova, O. I. *Phys. Rev. E* **2003**, *67*, 056313.

(7) Tretheway, D. C.; Meinhart, C. D. *Phys. Fluids* **2002**, *14*, L9–L12.

(8) Choi, C.-H.; Johan, K.; Westin, K. J.; Breuer, K. S. *Phys. Fluids* **2003**, *15*, 2897–2902.

(9) Joly, L.; Ybert, C.; Bocquet, L. *Phys. Rev. Lett.* **2006**, *96*, 046101.

(10) Lauga, E.; Brenner, M. P.; Stone, H. A. *Handbook of Experimental Fluid Dynamics*; Foss, J., Tropea, C., Yarin, A., Eds.; Springer: New York, 2005; Chapter 15.

(11) Neto, C.; Evans, D. R.; Bonaccorso, A.; Butt, H. J.; Craig, V. S. *Rep. Prog. Phys.* **2005**, *68*, 2559–2897.

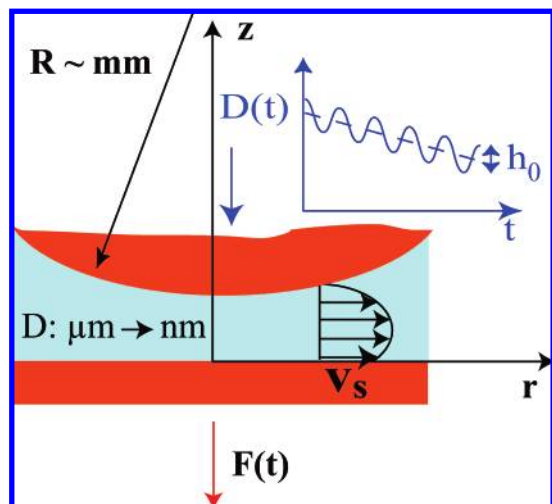


**Figure 1.** Schematic illustration of the flow between a sphere and a plane, with a no-slip boundary condition on the sphere and a partial-slip boundary condition on the plane.

We recall here the main properties of this drainage flow and how it allows the derivation of the boundary condition.

In a liquid, a sphere of radius  $R$  (about 3 mm) is located at a separation  $D$  from the plane such that  $D \ll R$  ( $D$  ranges from a few micrometers down to nanometers), and it is moved in its normal direction at velocity  $\dot{D}$  (Figure 1). This geometry accounts more generally for two curved surfaces of respective mean curvature  $1/R_1$  and  $1/R_2$  with  $R = R_1 R_2 / (R_1 + R_2)$ . The motion of the sphere squeezes the fluid out of ( $\dot{D} < 0$ ) or into ( $\dot{D} > 0$ ) the smallest gap region. We are interested here in fluid thicknesses large enough for macroscopic hydrodynamics to hold. This is obtained if the separation is larger than twice the interfacial region at the liquid/solid interface where the fluid structure deviates from its bulk properties, i.e., if  $D$  is larger than 6–10 molecular layers for the simple liquids considered here.<sup>12,13</sup>

The thickness-averaged velocity  $u(r)$  of the flow at distance  $r$  of the sphere–plane axis is obtained from volume conservation assuming that fluid compressibility effects and surface deformation are negligible. This averaged velocity  $u(r) = r\dot{D}/(2D + r^2/R)$  goes through a maximum at  $r = \sqrt{2RD}$  and decays as  $r^{-1}$  at larger distance.<sup>2</sup> Thus, the flow probes a surface area extending over a size  $\sqrt{2RD}$  normal to the sphere–plane axis. This probe size varies with the sphere–plane separation.

Under usual operating conditions of SFA and AFM, the Reynolds number of the flow,  $Re = \rho\dot{D}\sqrt{RD}/\eta$  with  $\rho$  being the liquid density and  $\eta$  being its viscosity, is low. The flow is purely viscous and can be described as a lubrication flow to good approximation. Relevant hydrodynamic quantities are the maximum pressure  $P_{\max}$  obtained on the sphere–plane axis, the maximum shear rate at the wall  $\dot{\gamma}_{\max}$ , and the overall viscous force exerted by the flow on the surfaces. In the case of a no-slip boundary condition on both surfaces, in the lubrication approximation these quantities are<sup>2</sup>

$$\begin{aligned} P_{\max} &= -\frac{3\eta R\dot{D}}{D^2}\left(1 + o\left(\frac{D}{R}\right)\right) \\ \dot{\gamma}_{\max} &= 1.38\dot{D}\sqrt{\frac{R}{D^3}}\left(1 + o\left(\frac{D}{R}\right)\right) \\ F &= -\frac{6\pi\eta R^2\dot{D}}{D}\left(1 + o\left(\frac{D}{R}\right)\right) \end{aligned} \quad (2)$$

They all vary with the sphere–plane separation. In the limit of  $D/R < 10^{-4}$  obtained in the following experiments, the Brenner correction<sup>14</sup> to the Reynolds force  $6\pi\eta R^2\dot{D}/D$  is less than a few  $10^{-4}$ ,

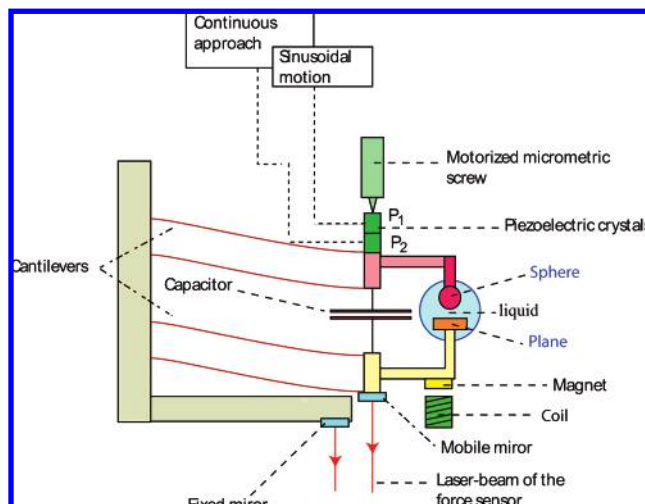


**Figure 2.** Schematic illustration of the dynamic surface force apparatus.

so only the lowest-order term of the viscous force is considered in the data analysis.

In the case of a partial-slip boundary condition, the flow between the sphere and the plane has been solved by Vinogradova.<sup>15</sup> The scaling laws (eq 2) still give an adequate order of magnitude for the relevant hydrodynamic quantities and can be used to estimate the maximum pressure and shear rate of the flow. For a partial-slip bc on only one of the surfaces (in the following experiments there is always a no-slip boundary condition on the sphere), the viscous force exerted by the flow is to lowest order in  $D/R$

$$\begin{aligned} F &= -\frac{6\pi\eta R^2\dot{D}}{D}f^*(\frac{b}{D}) \\ f^*(\frac{b}{D}) &= \frac{1}{4}\left(1 + \frac{3D}{2b}\left[\left(1 + \frac{D}{4b}\right)\ln\left(1 + \frac{4b}{D}\right) - 1\right]\right) \end{aligned} \quad (3)$$

It must be emphasized that this expression is valid only if the slip length  $b$  is uniform and independent of the shear rate. Thus, the linearity of  $F$  with velocity  $\dot{D}$  has to be checked before using eq 3 to derive a slip length from a measured viscous force. Another important point is that the viscous force depends on the boundary condition only through the factor  $f^*$ , which varies very smoothly with the slip length, from  $f^* \approx 1$  at  $b \ll D$  to  $f^* \approx 1/4$  at  $b \gg D$ . Therefore, to derive the slip length from the measured viscous force, the Reynolds viscous force must be estimated accurately. We discuss in more detail our data analysis procedure to derive the slip length from the measured viscous force in section 2.3.

**2.2. Dynamic Surface Force Apparatus.** Our dynamic surface force apparatus (DSFA, see Figure 2) is specifically designed to investigate the nanorheology of confined liquids.<sup>16</sup> For a given sphere–plane separation, flow is induced between the surfaces using a dynamic excitation: the sphere oscillates in the direction normal to the plane at a small amplitude  $h_0$  (ranging from 0.1 to 2 nm) and at a frequency  $\omega/2\pi$  that is tunable between 10 and 100 Hz. Thus, the driving velocity  $\dot{D}$  entering in eq 3 is harmonic, and its amplitude is  $h_0\omega$ .

Two subnanometer, time-resolved sensors measure independently the relative sphere–plane displacement and the force acting on the plane.

(12) Christenson, H. K.; Gruen, D. W. R.; Horn, R. G.; Israelachvili, J. N. *J. Chem. Phys.* **1987**, *87*, 1834–1841.

(13) Klein, J.; Kumacheva, E. *Science* **1995**, *269*, 816–819.

(14) Happel, J.; Brenner, H. *Low Reynolds Number Hydrodynamics*; Prentice-Hall: Englewood Cliffs, NJ, 1965.

(15) Vinogradova, O. I. *Langmuir* **1995**, *11*, 2213–2220.

(16) Restagno, F.; Crassous, J.; Charlaix, E.; Cottin-Bizonne, C.; Monchanin, M. *Rev. Sci. Instrum.* **2002**, *73*, 2292–2297.

The relative sphere–plane displacement is measured by a capacitive sensor whose plates are rigidly mounted on the cantilevers supporting the sphere and the plane. The quasi-static component (low-pass-filtered signal) gives the average relative displacement with a resolution of 1 Å. The amplitude  $h_o$  and the phase of the harmonic component at the excitation frequency are measured by a double lock-in amplifier with a dynamic resolution of 0.1 Å/√Hz.

The force acting on the plane is measured via the displacement of the cantilever on which it is mounted, by a Nomarski interferometer. The component of this displacement at the excitation frequency is also analyzed with respect to amplitude and phase by a second lock-in amplifier. The force  $F_\omega$  acting on the plane is then deduced using the force response of the cantilever, which is determined separately with an HP signal analyzer. With the cantilever spring constant  $k = 7200 \pm 90$  N/m used in the experiments reported here, and taking into account the noise level of the environment, a resolution of 40 nN/√Hz is achieved for the dynamic force in the frequency range of 10–100 Hz.

These two independent force and displacement measurements allow an accurate determination of the complex dynamic force response  $G_\omega(D) = F_\omega/h_o$ . The real part of this force response reflects elastic or potential interactions between the surfaces; it is zero for an incompressible Newtonian liquid between noninteracting rigid surfaces. The imaginary part  $G''_\omega$  is the dissipative component due to the viscous force exerted by the flow. To determine the boundary condition,  $G''_\omega$  is measured as a function of the sphere–plane separation  $D$  and compared to eqs 2 and 3 (replacing  $\dot{D}$  by  $h_o\omega$ ). For this purpose, the sphere is displaced at a very slow constant velocity (typically 5 Å s<sup>-1</sup>) toward and away from the plane. Performing several successive cycles of approaches and separations in each experiment allows us to evaluate the thermal drift of the measured separation and to correct it. The absolute value of the separation between the surfaces is determined from the contact position, located within 2 nm from the onset of the strong repulsive quasi-static force when the surfaces come into contact. The linearity of the hydrodynamic bc is easily probed by changing the excitation amplitude  $h_o$  or the excitation frequency  $\omega/2\pi$ . A linear bc corresponds to a response function  $G_\omega(D)$  independent of  $h_o$  and a damping  $G''(D)$  proportional to  $\omega$ .

**2.3. Data Analysis and Determination of the Boundary Condition.** As mentioned in section 2.1, a direct calculation of the slip length from the measured damping using eq 3 requires an accurate estimation of the Reynolds damping  $6\pi\eta R^2\omega/D$ . For this, values of the liquid viscosity  $\eta$  and of the sphere radius  $R$  have to be provided independently, and any error in them propagates badly onto the value of  $b$  because  $f^*$  is weak function of  $b$ . An even more serious drawback of this method is due to the divergence of the Reynolds force when  $D$  goes to zero. As a consequence, any offset error in  $D$  can lead to very large errors in the slip length. Both of these effects are demonstrated in section 5.1.

To avoid these drawbacks, we take advantage of the asymptotic expansion of eq 3 in the limit of large separation  $D \gg b$ :

$$F_v(D \gg b) \approx -\frac{6\pi\eta R^2 \dot{D}}{D+b} \quad (4)$$

At large separation, the viscous force is equivalent to the Reynolds force that would be obtained if the surfaces were distant from  $D + b$  instead of  $D$ . We use this property and analyze the data by plotting the inverse of the damping,  $G''^{-1}$ , as a function of the separation. The main features of this representation are illustrated in Figure 3, where the inverse of the dimensionless theoretical damping  $6\pi\eta R^2\omega h_o/b F_v = D/b f^*$  is plotted as a function of  $D/b$ . At large separations, the asymptotic expansion (eq 4) corresponds to a straight line of slope 1, whose extrapolation intersects the  $x$  axis at separation  $D/b = -1$ . For instance, at  $D/b = 10$  the tangent of the plot retrieves the value of the asymptotic slope to within 0.7%, and its intercepts with the  $x$  axis retrieves the value of  $D/b = -1$  to within 17%. We use this feature to determine the bc quantitatively. We first determine the value of the product  $\eta R^2$  from the slope of the curve  $G''^{-1}$  versus  $D$  at large separation, as well as a first estimate of  $b$ , and then we

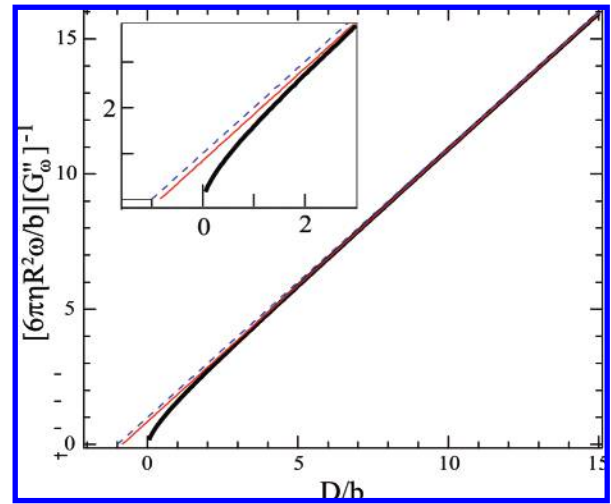


**Figure 3.** Continuous black curve: inverse of the dimensionless theoretical damping with a partial-slip bc on the plane as a function of the dimensionless sphere–plane separation  $D/b$ , according to eq 3. At short separation, the theoretical plot curves down and intersects the  $x$  axis at  $D/b = 0$ . Dashed line: asymptotic behavior at large separation derived from eq 4. It is a straight line of slope 1 that intercepts the  $x$  axis at a negative separation  $D/b = -1$ , giving the slip length  $b$ . Continuous thin line: tangent to the inverse of the dimensionless theoretical damping vs  $D/b$  at  $D/b = 10$ . Inset: enlargement around the origin. This tangent retrieves the slope of the asymptote to within 0.7% and the value of its intersection with the  $x$  axis to within 17%.

fit the data with eq 3 over the whole separation range, adjusting for the value of  $b$ . We finally check that the value obtained for  $\eta R^2$  is coherent with the measured sphere radius and the tabulated value of the liquid viscosity at the operating temperature. This method avoids introducing into the data analysis external values of parameters that are determined with a lower relative precision than the precision provided by the experimental setup. Another important advantage of this representation is that any experimental error in the origin of the absolute separation  $D$  results essentially in a translation of the  $D$  axis, and the same offset error in the determination of  $b$ , without the large amplification effects described in section 5.

Finally, this representation is helpful in detecting the presence of contamination by particles. As shown in Figure 3, the inverse of the theoretical damping curves down at small distance and intersect the  $D$  axis at the origin. The theoretical origin is defined as the contact between the mathematical surfaces where the bc applies. This is a very useful feature because in our experiments the origin of separations is determined from the quasi-static force at contact. Any difference in the position of these two origins reflects that the contact between the two surfaces does not occur in the average surface position experienced by the flow over the probed area. This is typical of contamination by particles (Figure 4). As a result, we reject any experiment where the inverse of the damping does not reach zero at  $D = 0$ . Note that because we are performing our experiments in a clean room and we follow the cleaning procedures detailed in the next section, most of the experiments for each system show an inverse of the viscous damping that tends to zero when separation  $D$  tends to zero.

### 3. Materials

We have investigated the flow of two liquids over a range of surfaces of varying nature and wettability. The two liquids are ultrapure water (Millipore, Milli-Q, 18.2 MΩ·cm) and a nonpolar liquid, *n*-dodecane (Aldrich) used as obtained. To study the influence of the liquid viscosity on the boundary conditions, we have also used water–glycerol mixtures prepared with ultrapure water and glycerol (Aldrich). The viscosities of the solutions are measured directly from the nanorheology experiments as described in section 2.3.

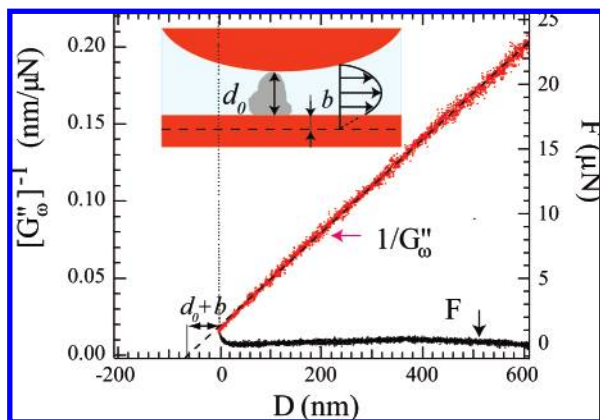


**Figure 4.** Typical results obtained in the case of contamination by particles, here for a water–glycerol mixture between an OTS-coated plane and a Pyrex sphere. Black dots: quasi-static force  $F$  as a function of separation  $D$ . The origin at the separation  $D = 0$  is set by the mechanical contact between the sphere and the plane, which occurs on a contaminating particle of height  $d_0$ . Red dots: inverse of viscous damping as a function of separation  $D$ . The inverse of viscous damping does not tend to zero when  $D$  tends to zero. Its asymptote (dashed line) intersects the  $D$  axis at a distance of  $D = -(d_0 + b)$  from the origin.

**Table 1. Contact Angles of the Different Systems Studied**

system	contact angle (deg)	hysteresis (deg)
OTS-Pyrex/water	105	2
DPPC monolayer/water	95	10
OTS-Pyrex/dodecane	28	2
Pyrex/water	<3	
Pyrex/dodecane	<3	
silicon/dodecane	4	3

All of the surfaces are prepared with a well-defined procedure summarized below. For each type of surface/preparation procedure, the generic properties are first characterized on samples that are not used for DSFA experiments. Nanorheology experiments are then performed on freshly prepared samples. The samples are mounted on the DSFA just after being prepared and are immediately dipped into a beaker containing the investigated liquid. All of DSFA experiments are performed in a clean, thermally isolated room.

On each type of surface, the following properties are measured. The results are gathered in Table 1.

(i) Wettability: The contact angle (advancing value and hysteresis) of the liquids studied is measured with a sessile drop method.

(ii) Roughness: The peak-to-peak value is extracted from an atomic force microscopy topographic image obtained in contact mode (AFM, Explorer Veeco) over a  $1 \mu\text{m} \times 1 \mu\text{m}$  area. On plain Pyrex samples, additional characterization has been performed by X-ray reflectometry.

(iii) Residual Contamination by Particles: This characteristic is very important for DSFA experiments because the measurement of the sphere–plane separation involves the determination of the origin from the contact force between the surfaces. We check for residual particle contamination by performing several large-area scans ( $100 \mu\text{m} \times 100 \mu\text{m}$ ) with the AFM. The probability of hitting one particle of height  $y$  in a DSFA experiment is  $p(y) = 2\pi R n(y)$ ,  $n(y)$  being the number of such particles per unit surface. In practice, we check that the preparation procedure does not lead to more than one particle of height 10 nm or larger over a  $100 \mu\text{m} \times 100 \mu\text{m}$  area. The probability of failure of a DSFA experiment is then less than 5%. Furthermore, as shown

in section 2.3, an experiment failing because of contamination by a particle is easily detected from the nanorheology data. Finally, with the preparation procedure and the protocol used, we can exclude in the following the presence of contaminating particles larger than 1 nm (0.5 nm for silicon surfaces) as well as the presence of molecular contamination in an amount sufficient to modify the wetting properties (contact angle or hysteresis) of the surfaces.

The surfaces are prepared as follows.

**Probes:** All spheres are made out of commercial Pyrex cylinders of 6 mm diameter, with an identical procedure. The end of the cylinder is fused in an oxygen–acetylene flame so as to obtain a sphere of radius typically between 2.8 and 3.4 mm. The sphere is then washed in an ultrasonic bath with a detergent (Micro90 for 30 min) and ultrapure water and then thoroughly rinsed with ultrapure water. The roughness is comparable to the roughness of Pyrex planes (described below). The contact angles of liquids on the spheres are not directly measured; they are assumed to be comparable to those measured on Pyrex planes.

**Pyrex Planes:** They are obtained from commercial Pyrex (Pignat, Lyon) using the same preparation procedure as for the spheres (except for the fusing). The roughness of the cleaned Pyrex planes is 1 nm peak-to-peak with a 0.7 nm rms. Both water and dodecane wet the Pyrex surfaces.

**OTS-Silanized Pyrex Planes:** The Pyrex surfaces are first cleaned as described above. They are then immersed in a mixture of 100  $\mu\text{L}$  of octadecyltrichlorosilane (Aldrich) and 60 mL of toluene for about 1 h in a low-humidity environment. They are then thoroughly rinsed with chloroform and finally with purified propanol. The quality of the SAM obtained is checked by the contact angle with water: this latter is at least  $105^\circ$ , with an hysteresis of at most  $2^\circ$ . The AFM topography of the surface prepared with this procedure is very similar to that of uncoated Pyrex planes, but with a slightly larger roughness (1 nm rms).<sup>17</sup>

**Silicon Planes:** Silicon samples, protected by a polymer film, are cut with a wafer saw. To remove organic and particulate contamination, they are immersed for 10 min in a piranha solution made of a 3:1 v/v mixture of sulfuric acid solution ( $\text{H}_2\text{SO}_4$ , 98%) and oxygen peroxyde solution ( $\text{H}_2\text{O}_2$ , 30%) at a temperature of  $120^\circ\text{C}$ . The samples are rinsed in deionized ultrapure water for 10 min at room temperature and then immersed in a hydrofluoric acid solution (HF, 49%). This procedure, called HF last in microelectronics, removes the particle contamination resulting from the cutting procedure. The first step (piranha) removes the organic contamination and a few of the contaminant particle by etching the native oxide layer in the silicon surface, and generates at the same time a new thin oxide layer of 0.8 nm.<sup>18</sup> The second step removes the remaining particles by etching the oxide layer. The roughness of the samples is 0.16 nm rms and 0.75 nm peak-to-peak over a  $1 \mu\text{m} \times 1 \mu\text{m}$  area.

**Phospholipid Monolayer on Pyrex:** DPPC monolayers (dipalmitoylphosphatidylcholine, Aventi Polar Lipids) are deposited on Pyrex planes at high lateral pressure by the Langmuir–Blodgett method. For this purpose, they are first formed in a Langmuir trough by spreading a millimolar solution of DPPC in chloroform–ethanol (9:1 v/v) on the surface of ultrapure water, before being transferred onto the Pyrex surfaces at a surface pressure of 40 mN/m after evaporation of the solvent.<sup>19</sup> The monolayers obtained are stable in air, with a uniform surface coverage and

(17) Cottin-Bizonne, C.; Cross, B.; Steinberger, A.; Charlaix, E. *Phys. Rev. Lett.* **2005**, *94*, 056102.

(18) Tardif, F.; Chabli, A.; Danel, A.; Rochat, N.; Veillerot, M. J. *Electrochem. Soc.* **2003**, *150*, G333–G338.

(19) Cross, B.; Steinberger, A.; Cottin-Bizonne, C.; Rieu, J. P.; Charlaix, E. *Europhys. Lett.* **2006**, *73*, 390–395.

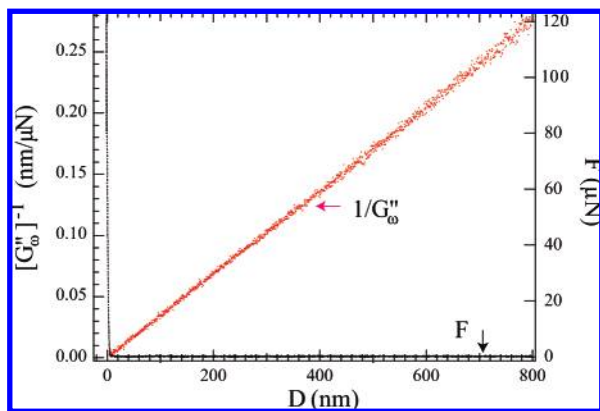


**Figure 5.** Red dots: inverse of the damping as a function of the separation  $D$  between the surfaces measured for a water–glycerol mixture between two Pyrex surfaces. The behavior corresponds to the Reynolds theory (i.e., a straight line going through the origin). This result is typical of those obtained in wetting systems. Black dots: quasi-static force as a function of  $D$ .

roughness of 2 Å rms, which is comparable to the values for the underlying Pyrex plane. They are hydrophobic: the advancing contact angle of water is 95° with a hysteresis of 10°. In water, the structure of the monolayers evolves slowly in time because of lipid reorganization.<sup>19</sup> After 2 h of hydration, the peak-to-peak roughness becomes 3 nm (i.e., comparable to the monolayer thickness). The nanorheology experiments are performed within this time delay after immersion in water.

#### 4. Properties of Boundary Flow

**4.1. General Behavior.** All of the results share the following properties.

First, the force responses measured are purely imaginary and do not show a significant real part except at separations very close to the contact ( $D < 5$  nm). This confirms that the rigid surface approximation holds (i.e., surfaces are not deformed significantly by the flow pressure). For the experiments with water–glycerol solutions, the absence of a real part also confirms their purely Newtonian character at the frequencies used.

All of the liquids used, including the water–glycerol mixtures, show a pure Reynolds damping when confined between two Pyrex surfaces (the typical result in Figure 5). In the experiments on Pyrex, the inverse of the damping is a straight line going through the origin over the whole range of separations investigated. This confirms that macroscopic fluid dynamics can be used for those liquids in the range of separations investigated here. Another important consequence of this result is that the boundary condition on the Pyrex sphere is a no-slip boundary condition in all subsequent experiments for all liquids, validating the use of eq 3 for data analysis.

Finally, the force responses measured are always linear and do not depend on the excitation amplitude  $h_0$ . This latter parameter is varied between 0.1 and 2 nm and is always kept lower than  $D/10$ . This rules out any nonlinear boundary condition such as slip effects depending on shear rate, in the limit of the low shear rates investigated here (maximum value of about  $5 \times 10^3$  s<sup>-1</sup>).

**4.2. Boundary Flow as a Function of Solid/Liquid Interactions.** *Perfectly Wetting and Partially Wetting Systems.* The main result is that we do not observe any significant slip effect on wetting systems. A no-slip boundary condition is obtained for all liquids on Pyrex and on the silicon surfaces (i.e., in perfectly wetting situations). No-slip flow is also observed for dodecane on OTS-coated Pyrex, which corresponds to a partial wetting condition (contact angle 28°). The uncertainty in this no-slip

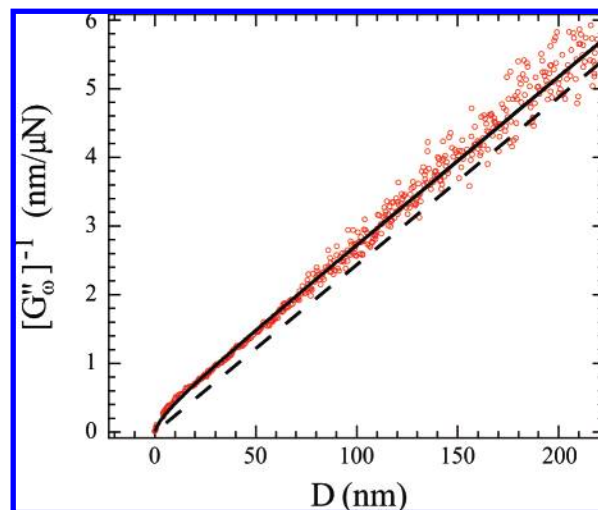


**Figure 6.** Inverse of damping  $G''^{-1}$  as a function of separation  $D$ , obtained for a water–glycerol solution on an OTS-coated Pyrex surface at a frequency of  $f = 69$  Hz. The black curve correspond to the theoretical expression for a slip length of  $b = 13$  nm. The dashed line corresponds to the inverse of damping in the case of no slip; it intersects the  $D$  axis at the origin.

boundary condition is 2 nm and is limited by the experimental determination of the contact position of the surfaces. Thus, we could not distinguish here an eventual small slip effect of dodecane on the OTS-coated Pyrex of less than 2 nm in amplitude. We also cannot rule out the possibility of a thin liquid layer being immobile at the wall (negative slip length). Finally, as stated before, this no-slip boundary condition does not change with the amplitude or shear rate in the limit of the investigation range (i.e., no onset of slip is detected at the largest shear rate).

*Strongly Hydrophobic Systems.* A well-defined partial-slip boundary condition is found solely on strongly nonwetting systems. For all systems, this partial-slip boundary condition corresponds to a constant, well-defined slip length. This property is necessary for using theoretical eq 3 to determine this slip length.

Figure 6 illustrates the case of a glycerol solution on OTS-coated Pyrex. The inverse of the measured damping is in very good agreement with the theoretical damping over the whole range of separations investigated. At large separation, its asymptotic behavior is a straight line whose slope gives the value of the viscosity of the solution ( $\eta = 2.8 \pm 0.2$  mPa s; the error bar is mainly due to the error bar on the measurement of the sphere radius,  $R = 1.35 \pm 0.05$  mm in this particular experiment). At shorter separations,  $G''^{-1}$  departs from its affine variation with  $D$  and curves down to intersect the  $D$  axis at its origin, in close agreement with the theoretical damping for  $b = 13 \pm 2$  nm. As discussed in section 2.3, this is an important feature because it shows that the surface position probed by the flow is identical to the surface position probed by the contact force. Thus, a constant finite slip length accounts for the damping from the largest separations (up to 200 nm), where the viscous damping vanishes into the noise, up to the shortest separations, where it reaches its maximum value. This constant slip length, which is not dependent on the shear rate or flow geometry for the whole range of separations measured, is an intrinsic characteristic of the L/S interface. The check for shear rate dependency has been made not only by changing the amplitude of the excitation but also by changing the frequency between 15 and 80 Hz. The amplitude of the slip effect found in those strongly nonwetting systems is moderate (below 20 nm) but fully resolved by the DSFA technique.

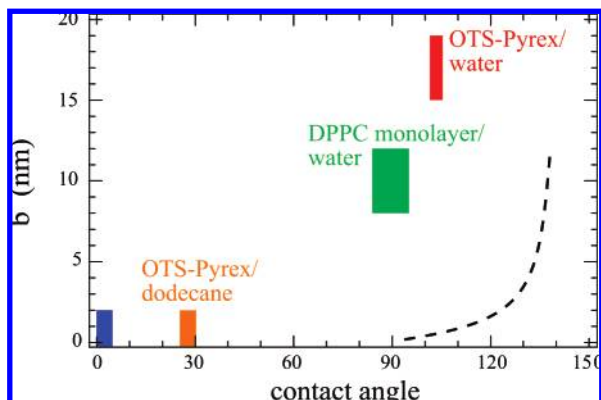


**Figure 7.** Slip length measured on various systems as a function of the liquid–solid contact angle. The blue rectangle corresponds to the values obtained for dodecane and water flowing on Pyrex and for dodecane flowing on silicon. The broken line corresponds to an interpolation of the values obtained with molecular dynamic simulations.

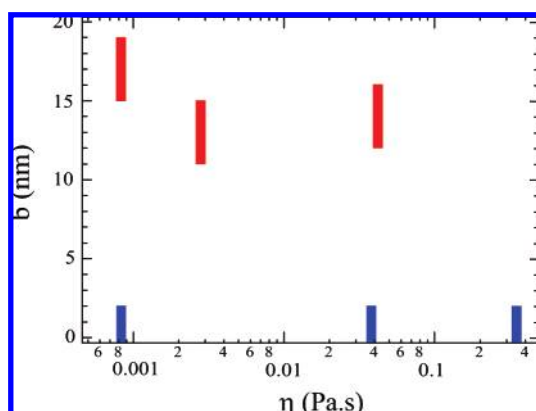


**Figure 8.** Slip length obtained for pure water and water–glycerol mixtures on Pyrex (blue) and OTS-coated Pyrex (red) as a function of their viscosity.

Figure 7 summarizes the slip lengths measured for the different systems as a function of the liquid–solid contact angle. On the two strongly nonwetting systems reported here, it is found that the slip length increases with the contact angle.

**4.3. Boundary Flow as a Function of Viscosity.** We used water–glycerol mixtures to investigate the effect of liquid viscosity on the boundary condition, with very weak changes in the wettability. Indeed for the water–glycerol mixtures used, the contact angle has a minor difference with that of water on Pyrex and OTS-silanized Pyrex, whereas the viscosities differ in a ratio of 50.

The results obtained (Figure 8) show that the slip length of the water–glycerol mixtures does not depend on their viscosity within the experimental uncertainty. Wettability is the major parameter controlling the occurrence and amplitude of the slip length.

## 5. Discussion

**5.1. Comparison with Other Dissipation Methods: The Importance of Data Analysis.** We first compare our results in more detail to the experimental studies of the boundary condition using the same method (i.e., the dissipation induced by drainage flow between a sphere and a plane).

Our results are consistent with a number of SFA and AFM studies investigating the flow of liquids wetting atomically smooth surfaces<sup>2,3,20,21</sup> or low-roughness surfaces.<sup>22,23</sup> The liquids are either nonpolar, water, or water solutions. Those studies all

indicate the presence of a no-slip boundary condition or a molecularly small negative slip length, i.e., a molecular layer of “immobile” liquid at a wall.

Our results are also in agreement with Vinogradova et al.’s investigation of water flow on hydrophobic polystyrene surfaces.<sup>24</sup> In this AFM study, a well-defined slip effect not depending on shear rate or sphere–plane separation is found, with an amplitude consistent with our data.

However, our results are not in agreement with other studies performed by SFA and AFM, both on wetting or nonwetting systems, that show rate-dependent slip effects. The rate effects reported are associated with changes in the sphere velocity and/or changes in the sphere–plane separation.<sup>25,26</sup> In some works, the existence of slip is found only above a critical shear rate, lying in the range of  $10^2$  to  $5 \times 10^3$  s<sup>-1</sup>, i.e. in the range of the shear rates investigated here. This is a significant difference with the present results because we find constant slip lengths over the whole range of shear rate investigated (between 10 and  $5 \times 10^3$  s<sup>-1</sup>). We also emphasize that the studies that claim a rate-dependent slip length (see, for example, the review in ref 11 or ref 26), actually use eq 3 to analyze their results, but as already mentioned, eq 3 is valid only when  $b$  is not rate-dependent.

Tentative explanations for this qualitative discrepancy mention the problem of surface control and contamination. Indeed, the surface topography and the presence of roughness even on a small scale are expected to play a major role in the flow boundary condition. Also, the presence of surfactant contamination and dissolved gas and the possible nucleation of small bubbles in surfaces holes have been suggested as a possible source of the shear-rate-dependency in the bc.<sup>10,11</sup>

We discuss here in more detail a specific source of apparent nonlinear effects in the boundary condition, which is related to minute experimental errors in the determination of the separation between the surfaces. The dramatic importance of an accurate determination of the separation between the confining surfaces has been experimentally demonstrated by Honig et al.<sup>23</sup> By implementing on AFM a light-diffusion technique allowing an absolute measurement of the probe–surface separation, they found a no-slip boundary condition on a liquid/solid system on which the rate-dependent slip effect had been previously observed with a more standard AFM technique.<sup>25</sup>

We demonstrate here that depending on the data analysis procedure, minute experimental errors in separation  $D$  can lead to a huge effect on the slip-length measurement. For this, we perform a gedanke experiment on a liquid–solid surface with an actual constant slip length  $b_{\text{real}} = 20$  nm. The first type of error considered in Figure 9 is an offset error on the measured separation: the actual sphere–plane separation is  $D_{\text{real}} = D_{\text{meas}} + D_{\text{off}}$ . The measured viscous force is thus  $F_{\text{meas}} = (6\pi\eta R^2 D / D_{\text{real}}) f^*(b_{\text{real}} / D_{\text{real}})$ . The experimental slip length  $b$  is then derived for each experimental point by inverting eq 3:  $f^*(b / D_{\text{meas}}) = F_{\text{meas}} D_{\text{meas}} / 6\pi\eta R^2 \dot{D}$ . Figure 9 shows that an error of 2 nm in the separation can result in an overestimation as large as one order of magnitude of the actual slip length. Furthermore, the apparent slip length increases when the separation decreases.

(20) Klein, J.; Kamiyama, J. J. Y.; Yoshizawa, H.; Israelachvili, J. N.; Fredrickson, G. H.; Pincus, P. L.; Fetters, J. *Macromolecules* **1993**, *26*, 5552–5560.

(21) Becker, T.; Mugele, F. *Phys. Rev. Lett.* **2003**, *91*, 166104.  
(22) Georges, J.-M.; Milliot, S.; Loubet, J. L.; Tonck, A. *J. Chem. Phys.* **1993**, *98*, 7345.

(23) Honig, C. D. F.; Ducker, W. A. *Phys. Rev. Lett.* **2007**, *98*, 028305.

(24) Vinogradova, O. I.; Yabukov, G. E. *Langmuir* **2003**, *19*, 1227–1234.

(25) Craig, V. S. J.; Neto, C.; Williams, D. R. M. *Phys. Rev. Lett.* **2001**, *87*, 054504.

(26) Zhu, S.; Granick, Y. *Phys. Rev. Lett.* **2001**, *87*, 096105.

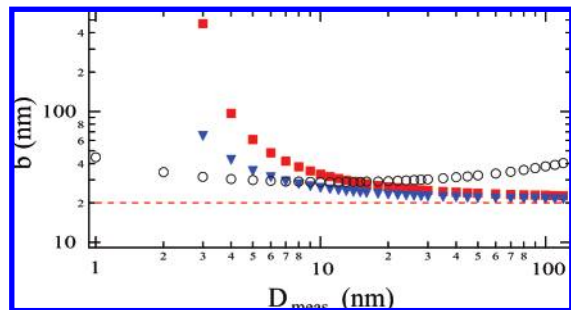


**Figure 9.** Effect of data analysis on the determination of the slip length. The real slip length is  $b_{\text{real}} = 20$  nm (dashed line). An experimental value of the slip length is derived from each measured value of the viscous force by inverting eq 3. (■) effect of an offset error of  $D_{\text{off}} = 2$  nm on the measured separation, (▼)  $D_{\text{off}} = 1$  nm, and (○) effect of an overestimation of 5% on the sphere radius.

Because the shear rate also increases for a given driving velocity  $\dot{D}$ , this effect could be wrongly attributed to a shear-rate-dependent boundary condition. Another type of error considered in Figure 9 is an overestimation of the sphere radius. Here, an experimental slip length is again derived for each experimental point by inverting eq 3:  $f^*(b/D) = f^*(b_{\text{real}}/D)R_{\text{real}}^2/R_{\text{meas}}^2$ . An overestimation of 5% of the sphere radius can lead to an overestimation of 100% of the slip length. This second type of error is less dependent on the sphere–plane separation.

Thus, data analysis is crucial to determining the boundary condition without a huge amplification of small experimental errors. In AFM, a small inaccuracy in the probe–surface separation can occur because of the determination of the contact position (as shown in ref 23). In classical SFA, the separation is directly measured by interferometry through the contact zone. However, in dynamic flows the oscillating elastohydrodynamic deformation of the glued mica surfaces has to be rigorously taken into account; otherwise, it may induce important errors in the slip length.<sup>27</sup> Our procedure for determining the slip length minimizes the propagation of separations errors in the slip length, as explained in section 2.3. Of course, this procedure reports the sensitivity to any measurement error on damping because the inverse of the damping is actually analyzed. However, such errors are important only at large separations, when viscous damping vanishes. We take great care in our experiments to characterize precisely all residual damping (i.e., other than the viscous force due to the flow between the sphere and the plane) by performing “white runs” in which the sphere is kept at very large separation from the plane.

**5.2. Comparison with Theory.** We now compare our experimental results to the theoretical predictions for the intrinsic boundary condition on smooth surfaces. The actual theoretical understanding of the hydrodynamic boundary condition of simple liquids on solid surfaces is issued from molecular dynamics simulations and statistical physics analysis of transverse momentum transfert. Early work by Robbins showed that the flow properties of simple Lenard-Jones liquids at a solid wall depend on the liquid organization parallel and transverse to the wall.<sup>28</sup> Subsequent work by Barrat et al.<sup>29</sup> quantify these tendencies with a phenomenological expression for the slip length as a function of structural parameters in the interfacial region

$$b \approx \frac{\sigma}{S_1(q)c_{\text{FS}}^2\rho_c\sigma^3}$$

where  $\sigma$  is the molecular size,  $\rho_c$  is the molecular fluid density at the wall,  $c_{\text{FS}}$  is a parameter giving the relative fluid/solid to fluid/fluid interaction energy (governing the contact angle), and  $S_1(q)$  is the structure factor of the first layer of liquid at the wave vector of the wall molecular corrugation. The slip length is found to be tightly related to the interaction parameter, which enters this expression both directly and through the density of the fluid. For a dense interfacial region, obtained under either wetting conditions or nonwetting conditions, at high pressure, one essentially has a no-slip boundary condition. For the nonwetting case at low pressure, a depletion layer appears at the wall, and partial slip is obtained. At a given pressure, the slip length increases with the contact angle as the depletion layer develops. We compare the theoretical results to our data for water by choosing an arbitrary value of  $3\text{ \AA}$  for the molecular size. The tendency reported for Figure 7 is in good agreement with our data obtained for water and dodecane on the various substrates. It also accounts for the absence of a viscosity effect on slip length observed with the water–glycerol mixtures, because the theoretical expression does not depend directly on any dynamic property of the liquid. However, the absolute amplitude of the slip length is much smaller than in the experiments.

A simple model assimilating the depletion layer to a gaseous film has been used by Doshi et al.<sup>30</sup> to estimate the intrinsic slip length. The authors measure the thickness of a depletion layer at the liquid–solid interface by neutron reflectivity and derive the slip length from the viscosity contrast between a gaseous phase and the bulk liquid. For OTS-grafted quartz in water, a system comparable to our coated Pyrex system, they find a 5 Å-thick depletion layer and derive a slip length of 25 nm. This magnitude is comparable to our results for water on strongly hydrophobic systems. However, because the slip length estimation in this gas layer model depends on the viscosity of the depletion layer, the result for the water–glycerol mixtures cannot be retrieved directly.

## 6. Conclusions

We have presented here an overview of the possibilities of dynamic surface forces for determining the intrinsic flow boundary condition of liquids on solid surfaces. We have discussed in detail the impact of experimental uncertainties and data analysis on the precision of the boundary flow characterization. We have investigated more specifically the behavior of two liquids, polar and nonpolar, on a variety of surfaces of low roughness. On all of the wetting systems investigated, we find that the no-slip boundary condition holds within 2 nm. We cannot rule out the existence of a liquid layer of molecular size trapped at the solid wall. On strongly hydrophobic surfaces, we show evidence of a well-defined partial slip of water characterized by a constant slip length accounting for the flow over a whole range of separation, liquid film thickness, and shear rate. The slip length increases with hydrophobicity but does not exceed 20 nm. These values match the ones measured on identical surfaces at zero shear rate with a different setup,<sup>9</sup> and we believe that they indeed represent an intrinsic boundary condition. Using water–glycerol mixtures of various viscosities, we also find that the boundary condition is essentially determined by surface interactions and depends little on the fluid viscosity.

(28) Thompson, P. A.; Robbins, M. O. *Phys. Rev. A* **1990**, *41*, 6830–6837.

(29) Barrat, J.-L.; Bocquet, L. *Faraday Discuss.* **1999**, *112*, 119–127.

(30) Doshi, D. A.; Watkins, E. B.; Israelachvili, J. N.; Majewski, J. *Proc. Natl. Assoc. Sci. U.S.A.* **2005**, *102*, 9458–9462.

(27) Steinberger, A.; Cottin-Bizonne, C.; Kleimann, P.; Charlaix, E. *Nat. Mater.* **2007**, *6*, 665–668.

These results for the intrinsic flow properties on smooth surfaces are of interest in microfluidics, either for amplifying interfacial transport phenomena<sup>1</sup> or for lowering hydrodynamic dispersion in separation devices.<sup>31,32</sup> Work is in progress to investigate the boundary flow on complex surfaces such as hydrophobic surfaces with nanometric roughness.

---

(31) Charlaix, E.; Hulin, J. P.; Leroy, C.; Lenorm, R.; Zarcone, C. *J. Phys. D: Appl. Phys.* **2005**, *21*, 1727–1732.

**Acknowledgment.** We thank L. Leger and R. Ober for helpful comments and the X-ray characterization of Pyrex surfaces. We gratefully acknowledge support from the ANR P-Nano.

LA7024044

---

(32) Eghbali, H.; Desmet, G. *J. Sep. Sci.* **2007**, *30*, 1377–1397.